

1. P.W.F. Alons, R.D. Bent, J.S. Conte and M. Dillig, Nucl. Phys. **A480** (1988) 413-468.
2. J.J. Kehayias, R.D. Bent, M.C. Green, M.A. Pickar and R.E. Pollock, Phys. Rev. **C33** (1986) 725.

## ENERGY DEPENDENCE OF THE ${}^3\text{He}(p,\pi^+){}^4\text{He}$ REACTION

R. D. Bent

*Indiana University Cyclotron Facility, Bloomington, Indiana 47405*

P. W. F. Alons

*Indiana University Cyclotron Facility, Bloomington, Indiana 47405  
and NIKHEF, P.O. Box 41882, 1009 DB Amsterdam, The Netherlands*

M. Dillig

*Institute for Theoretical Physics, University of Erlangen-Nurnberg  
Erlangen, W. Germany*

We have described previously our microscopic model<sup>1</sup> of proton-induced nuclear pion production and its application<sup>1,2</sup> to the  ${}^3\text{He}(p,\pi^+){}^4\text{He}$  reaction at  $T_p^{lab} = 200$  MeV. Recently, we have examined the *energy dependence* of the various components of the calculations from the near threshold region [ $T_p^{lab} = 178$  MeV,  $T_\pi^{cm} = 10.5$  MeV] to an energy at which the  $\Delta_{1232}$  resonance should clearly dominate the reaction mechanism [ $T_p^{lab} = 300$  MeV,  $T_\pi^{cm} = 93.6$  MeV]. The full calculations are compared with existing differential cross section and analyzing power data<sup>3</sup> at  $T_p^{lab} = 178$  and 200 MeV, and with cross section data<sup>4,5</sup> from the time-reversed  ${}^4\text{He}(\pi^-,n){}^3\text{H}$  and  ${}^4\text{He}(\pi^+,p){}^3\text{He}$  reactions at equivalent proton laboratory energies of 229, 262, 296 and 329 MeV, assuming charge symmetry and detailed balance. The only energy above 200 MeV at which *both* differential cross section and analyzing power data are available is 800 MeV<sup>6</sup>, far above the region of applicability of our model.

Our microscopic model of the  $A(p,\pi)A+1$  reaction is based on mesonic and isobaric degrees of freedom and includes explicitly both the one-nucleon mechanism (ONM) and the resonant p-wave rescattering part of the two-nucleon mechanism (TNM). Higher order processes are included through proton-nucleus and pion-nucleus optical-model distortions. For the present calculations, the proton distortions were obtained using optical model potentials that give a good description of proton elastic data at 178 MeV<sup>7</sup> and at 200 and 300 MeV<sup>8</sup>, and then interpolating for 250 MeV. The pion distorted waves were generated using the pion-nucleus optical model code DWPIES (which is described in Ref. 1) and including second-order parameters determined by systematic fits to a large body of  $\pi$ -elastic data<sup>9</sup>. The second-order parameters are well known up to only 80 MeV pion energy, so an extrapolation was required to obtain the parameters for  $T_p = 300$  MeV, which is equivalent to a laboratory pion energy of 103 MeV. An energy-dependent pion self-energy was included in the two-nucleon mechanism.

In Fig. 1 we compare our calculations at  $T_p = 178$  and 200 MeV with the data of Kehayias et al.<sup>3</sup>, which are in good agreement with the cross section data of Willis et al.<sup>10</sup> at  $T_p = 180$  and 201 MeV, and show the decomposition of the full calculations (solid lines) into the projectile-emission (PEM), target-emission (TEM) and one-nucleon mechanism (ONM) components. The corresponding calculations at  $T_p = 250$  and 300 MeV are also shown in Fig. 1. Presently, no analyzing power data are available at 250 and 300 MeV, but experiments covering this energy range have been proposed<sup>11</sup>). The model predicts a characteristic shift in the pattern of the analyzing power angular distributions between  $T_p = 178$  and 300 MeV; it would be interesting to see if these predictions are borne out by experiment. At 178 MeV the calculations are dominated by the (ONM) amplitude and reproduce the data remarkably well, except for an overall factor of 2.5 in the magnitude of the cross section. At 200 MeV the calculations agree less well with the data, perhaps because at this energy they are sensitive to the interference between two approximately equal amplitudes (ONM and PEM). Fig. 1 shows that the TEM amplitude is practically negligible at all energies.

It may seem surprising that the ONM contribution is so large and does not fall more rapidly at large angles, corresponding to large momentum transfers. In a *plane-wave* ONM calculation, the cross section is directly proportional to the high momentum components of the bound-state wave function and is indeed much smaller, and several orders of magnitude smaller at  $180^\circ$  than at  $0^\circ$  (see Ref. 1). In the present calculations, the curves labeled ONM include both proton distortions and *non-resonant* pion distortions, which help with the momentum sharing and raise significantly the cross sections, particularly at large angles.

The analyzing powers shown in Fig. 1 vary smoothly with energy. The PEM and TEM contributions individually give opposite signs for  $A_y$ , but TEM has little effect because of its very small cross section. The analyzing power is essentially that of the ONM at 178 MeV but is sensitive to the interference between the ONM and PEM contributions at the higher energies. Analyzing power data at higher energies would provide a particularly sensitive test of the model.

Fig. 2 displays the energy dependence of the full calculations and of the ONM, PEM and TEM contributions separately. In this figure, we plot the differential cross sections and analyzing powers versus the relativistically invariant Mandelstam variable  $t$ , which is the square of the four-momentum transfer. Comparing the cross sections at a constant  $t$ -value to minimize nuclear structure effects<sup>12,13</sup>, we see that the ONM cross section varies by only a factor of 4 between 178 and 300 MeV, whereas the PEM and TEM contributions vary by about 3 orders of magnitude over this energy range. Consequently, the ONM dominates the reaction at 178 MeV but PEM dominates at 250 and 300 MeV (at forward angles). The ONM analyzing powers also vary less rapidly with energy than the PEM and TEM analyzing powers.

Fig. 3 shows the effects of distortions at the various energies. Despite the fact that the dominant rescattering mechanism is included microscopically in our model, the 178 and 200 MeV calculations are still quite sensitive to distortions. The difficulties in describing the 200 MeV data may very well be due to shortcomings of the optical model distortions for such light systems<sup>2</sup>. The sensitivity to distortions is somewhat less at 250 and 300 MeV. It is seen from Fig. 3 that the analyzing powers are sensitive to *both* proton

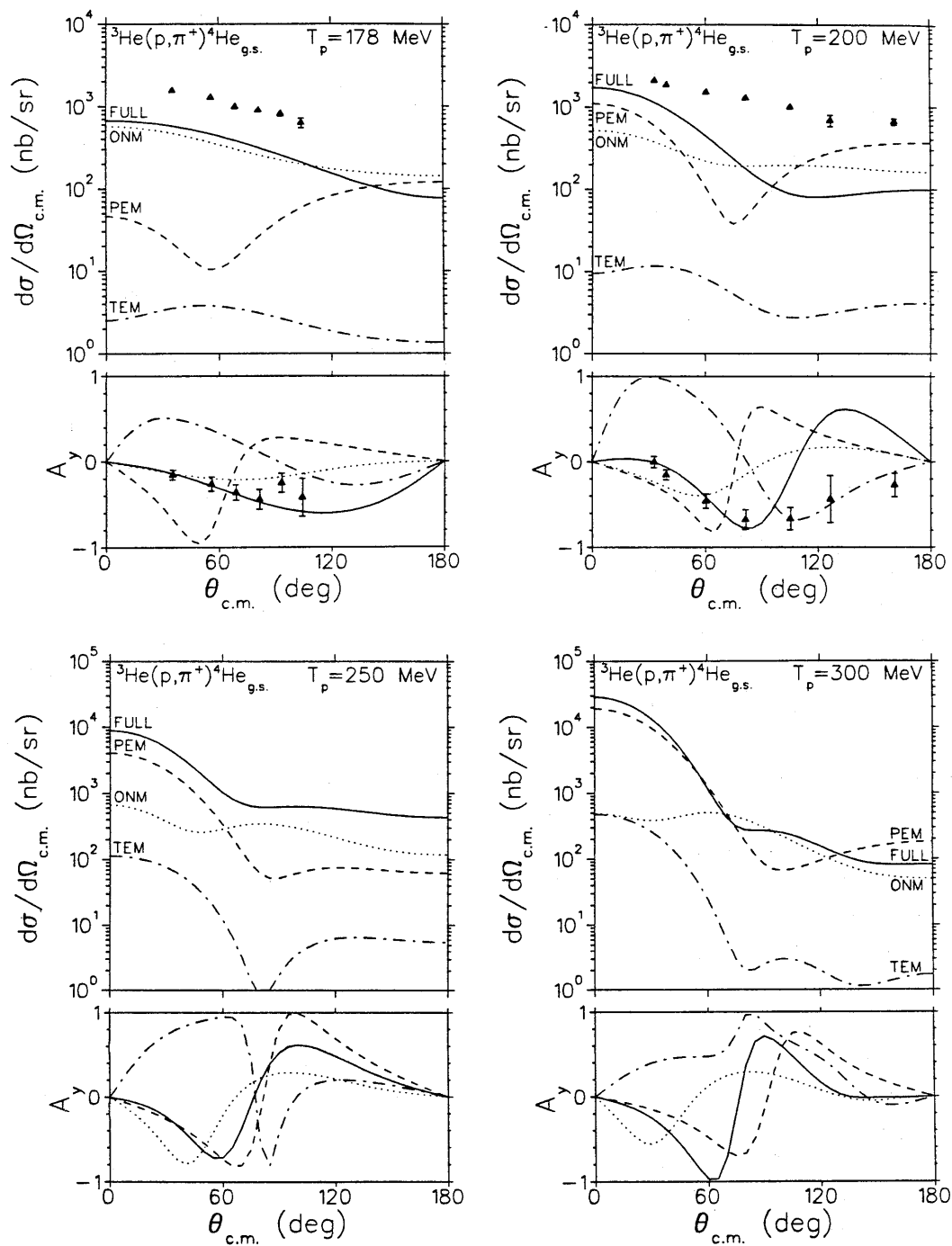


**Figure 1.** Decomposition of full TNM calculations (solid lines) of the  ${}^3\text{He}(p, \pi^+){}^4\text{He}_{g.s.}$  reaction into the one-nucleon mechanism (dotted lines), projectile-emission (dashed lines) and target-emission (dot-dashed lines) contributions, at  $T_p = 178, 200, 250$  and  $300$  MeV. The data are from Ref. 3.

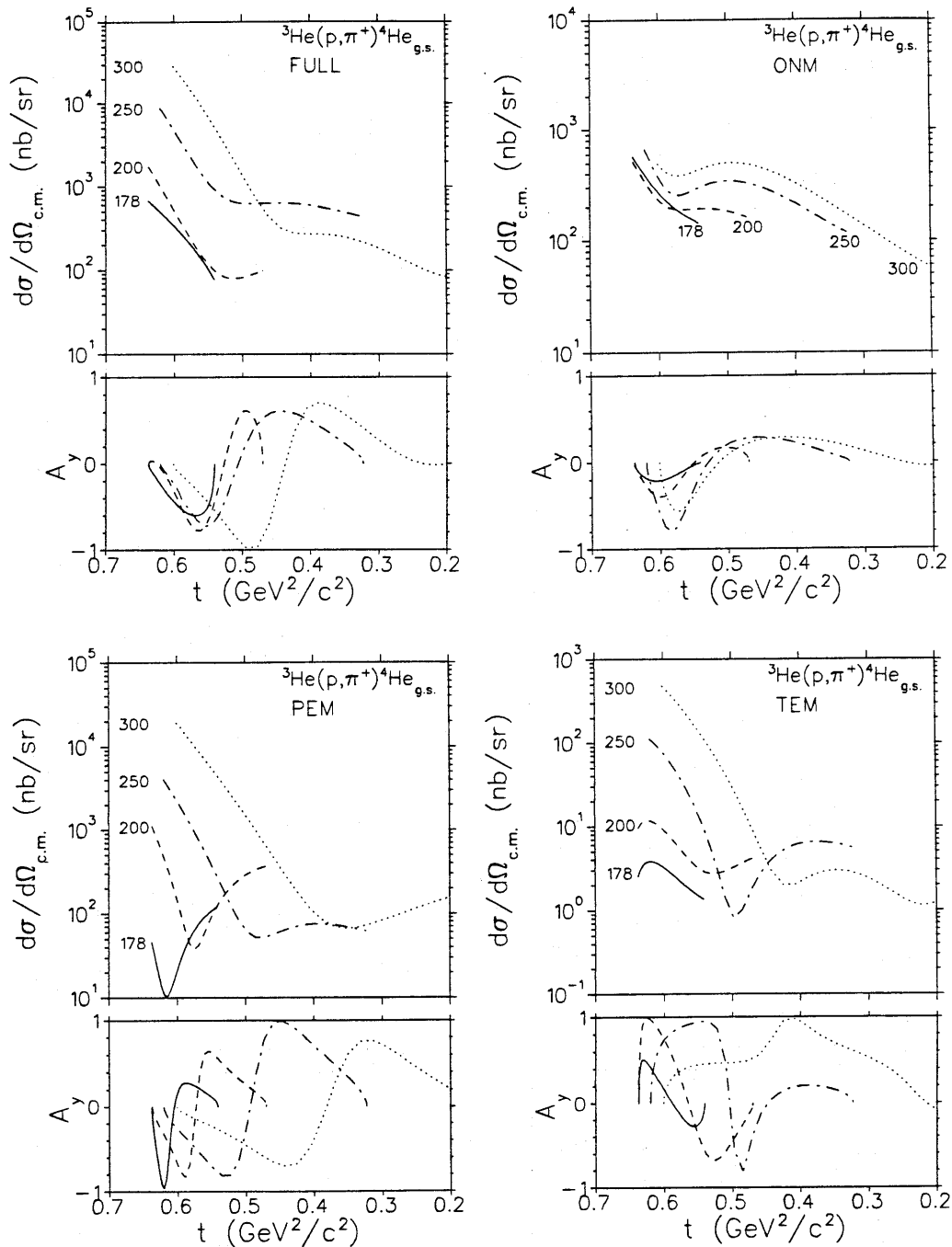
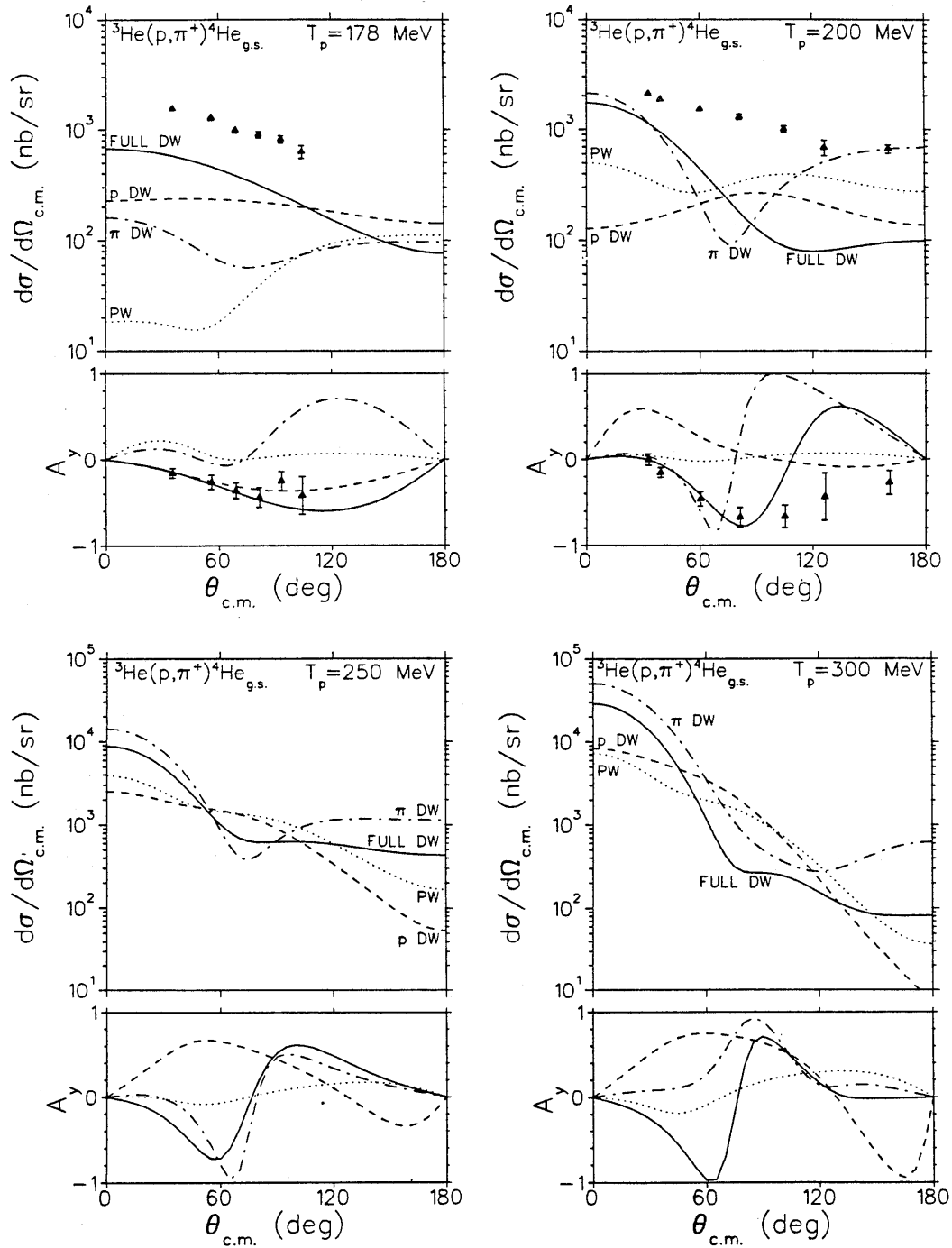


Figure 2. TNM calculations for the  ${}^3\text{He}(p, \pi^+){}^4\text{He}_{g.s.}$  reaction at  $T_p^{lab}=178$  MeV (solid lines), 200 MeV (dashed lines), 250 MeV (dot-dashed lines) and 300 MeV (dotted lines). The full (FULL) calculations represent the coherent sum of the one-nucleon mechanism (ONM), projectile-emission (PEM) and target-emission (TEM) contributions, which are also shown separately. The cross sections and analyzing powers are plotted versus the relativistically invariant Mandelstam variable  $t$ , which is the square of the four-momentum transfer.



**Figure 3.** TNM calculations for the  ${}^3\text{He}(p, \pi^+){}^4\text{He}_{g.s.}$  reaction at  $T_p^{lab} = 178, 200, 250$  and  $300$  MeV with plane waves (dotted lines), proton distortions only (dashed lines), pion distortions only (dot-dashed lines) and full distortions (solid lines). The data are from Ref. 3.

and pion distortions, which separately tend to give opposite signs for  $A_y$ . The effects of pion distortions are surprisingly large at the two lowest energies ( $T_p^{lab}=178$  and 200 MeV corresponding to  $T_\pi^{cm}=10.5$  and 25.7 MeV, respectively) considering that the  $\pi$ -nucleus interaction is weak at these energies, corresponding to a pion mean-free-path in nuclear matter<sup>14</sup> that is large compared to the size of the  ${}^4\text{He}$  nucleus. Pion distortions were ignored in some of the early calculations<sup>15,16</sup> of  $(p, \pi)$  analyzing powers, but were included in others<sup>17</sup>.

Although analyzing power data are not yet available to compare with the present calculations above 200 MeV, cross sections for the charge-symmetric, time-reversed reaction  ${}^4\text{He}(\pi^-, n){}^3\text{H}$  have been measured<sup>4</sup> at pion lab energies of 50, 75, 100, and 125 MeV (and higher energies). Fig. 4 shows these data transformed to the  $(p, \pi^+)$  reaction using detailed balance (top), together with the 178 and 200 MeV  ${}^3\text{He}(p, \pi^+){}^4\text{He}$  data of Kehayias et al.<sup>3</sup> (middle) and the present calculations made at close to the experimental energies (bottom). We note that the calculations predict a monotonic decrease in cross section with energy at large  $t$ -values, whereas the 200 MeV cross sections of Kehayias et al.<sup>3</sup> are larger than those at 229 MeV obtained from the 50 MeV  $(\pi^-, n)$  data of Källne et al.<sup>4</sup> by detailed balance.

Fig. 5 shows a comparison of the calculated  $(p, \pi^+)$  and transformed  $(\pi^-, n)$  cross sections. The calculations reproduce qualitatively the gross features of the angular distributions. The magnitudes of the calculated cross sections, however, are consistently *larger* than those obtained by detailed balance from the  $(\pi^-, n)$  data<sup>4</sup>, whereas they are *smaller* than the  $(p, \pi^+)$  cross sections measured<sup>3</sup> at  $T_p^{lab} = 178$  and 200 MeV (see Fig. 1).

Källne et al.<sup>5</sup> have also measured cross sections for the  ${}^4\text{He}(\pi^+, p){}^3\text{He}$  reaction at one angle ( $\theta_p = 20^\circ$ ) for  $T_\pi = 50$  and 100 MeV. They obtained cross sections that were larger than those obtained earlier from the  ${}^4\text{He}(\pi^-, n){}^3\text{H}$  reaction<sup>4</sup> by factors of 3.25 and 1.7, respectively, at the two energies.

In Fig. 6 the cross sections obtained from Fig. 4 at a constant four-momentum transfer of  $t = 0.575$  ( $\text{GeV}^2/c^2$ ) are plotted vs  $\sqrt{s} - m({}^3\text{He})$ , where  $s$  is the relativistic Mandelstam variable corresponding to the square of the center of mass energy. This quantity represents the energy available for excitation of one nucleon, e.g., to an intermediate  $\Delta_{1232}$ , in a two-nucleon mechanism<sup>12,13</sup>. Also plotted in Fig. 6 are the cross sections obtained from the 50 and 100 MeV  $(\pi^-, n)$  data<sup>4</sup> by detailed balance multiplied by 3.25 and 1.7, respectively, as indicated by the  $(\pi^+, p)$  data<sup>5</sup>. The calculations give about the right slope for the excitation function, falling in between the low energy  ${}^3\text{He}(p, \pi^+){}^4\text{He}$  data<sup>3</sup> and the higher energy  ${}^4\text{He}(\pi^-, n){}^3\text{H}$  data<sup>4</sup>, in rough agreement with the  ${}^4\text{He}(\pi^+, p){}^3\text{He}$  data<sup>5</sup>. New  ${}^3\text{He}(p, \pi^+){}^4\text{He}$  cross section data in the 200 – 300 MeV range would be helpful in resolving the discrepancies shown in Fig. 6.

In summary, our microscopic model describes fairly well the angular distributions of both the differential cross sections and the analyzing powers at  $T_p = 178$  and 200 MeV, and also gives qualitatively the correct energy dependence of the cross sections up to  $T_p = 325$  MeV. New experiments are needed to resolve discrepancies among existing  $(p, \pi^+)$ ,  $(\pi^-, n)$  and  $(\pi^+, p)$  cross section data and to obtain analyzing powers at the higher energies, which would provide stringent tests of the model.

1. P.W.F. Alons, R.D. Bent, J.S. Conte and M. Dillig, Nucl. Phys. **A480** (1988) 413-468.

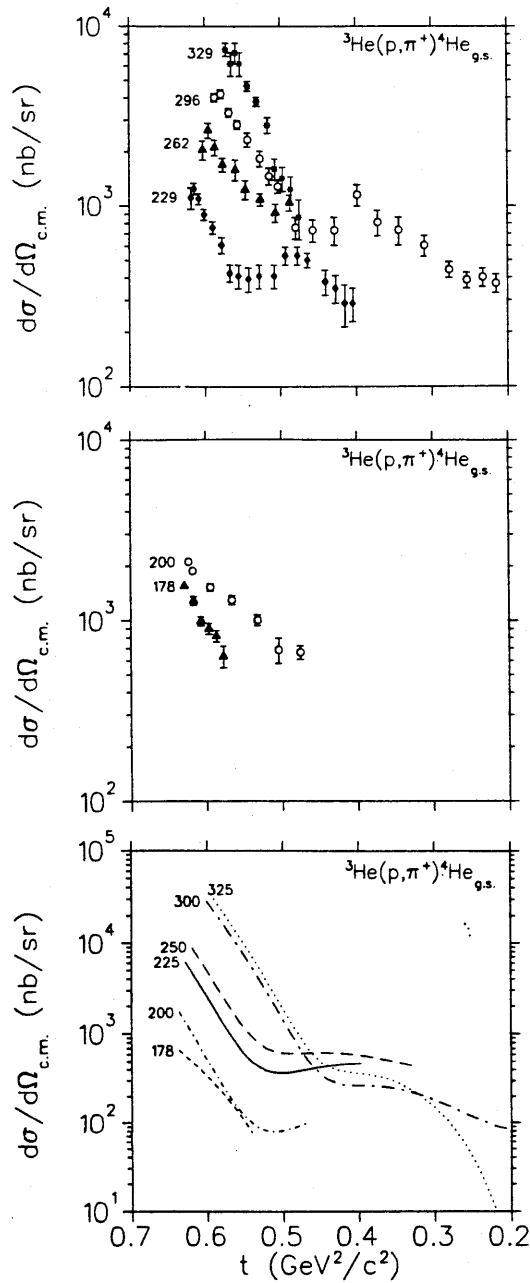


**Figure 4.** Top:  ${}^3\text{He}(p, \pi^+){}^4\text{He}_{g.s.}$  differential cross sections at  $T_p = 229, 262, 296$  and  $329$  MeV obtained from the  ${}^4\text{He}(\pi^-, n){}^3\text{H}$  data of Ref. 4 at  $T_\pi^{lab} = 50, 75, 100$  and  $125$  MeV by detailed balance. Middle:  ${}^3\text{He}(p, \pi^+){}^4\text{He}_{g.s.}$  differential cross sections at  $T_p = 178$  and  $200$  MeV from Ref. 3. Bottom: Calculated differential cross sections for the  ${}^3\text{He}(p, \pi^+){}^4\text{He}_{g.s.}$  reaction at  $T_p = 178, 200, 225, 250, 300$  and  $325$  MeV. The abscissa is the relativistically invariant Mandelstam variable  $t$ , which is the square of the four-momentum transfer.

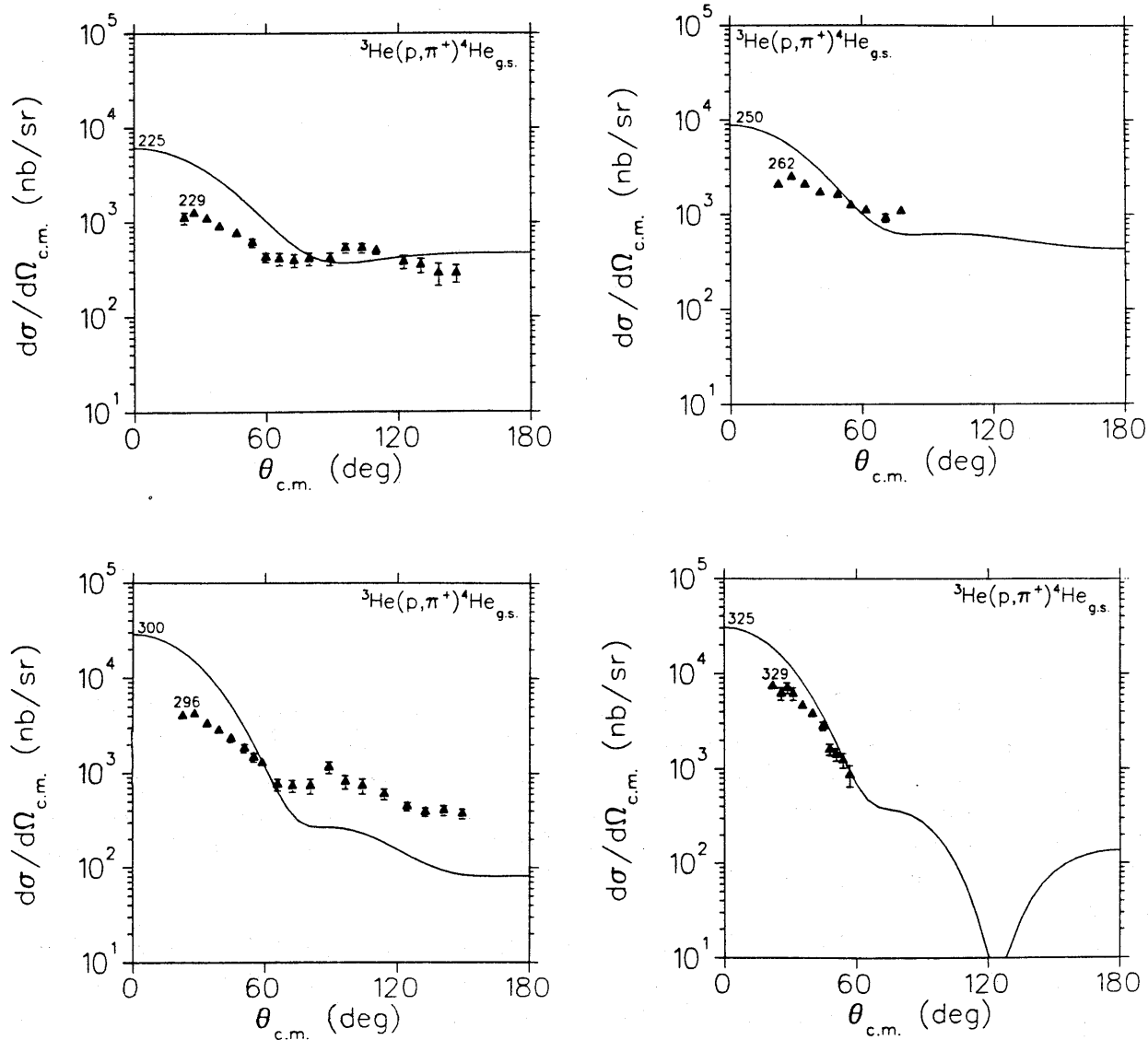


**Figure 5.** Comparison of calculated  ${}^3\text{He}(p, \pi^+){}^4\text{He}_{g.s.}$  differential cross sections at  $T_p^{lab} = 225, 250, 300$  and  $325$  MeV with experimental differential cross sections at  $T_p^{lab} = 229, 262, 296$  and  $329$  MeV obtained from the  ${}^4\text{He}(\pi^-, n){}^3\text{H}$  data of Ref. 4 at  $T_\pi^{lab} = 50, 75, 100,$  and  $125$  MeV by detailed balance.



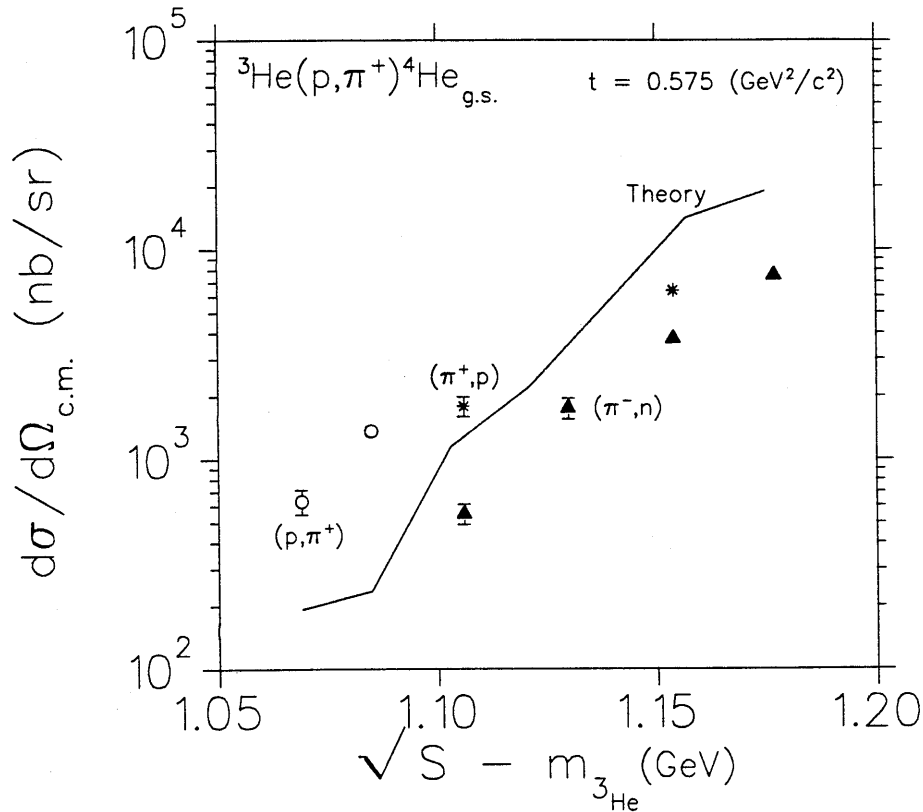


**Figure 6.** Energy dependence of the  ${}^3\text{He}(p, \pi^+){}^4\text{He}_{g.s.}$  differential cross sections at a constant four-momentum transfer of  $t = 0.575 \text{ GeV}^2/c^2$ . Open circles:  ${}^3\text{He}(p, \pi^+){}^4\text{He}_{g.s.}$  data from Ref. 3. Solid triangles:  ${}^4\text{He}(\pi^-, n){}^3\text{H}$  data from Ref. 4 transformed to  ${}^3\text{He}(p, \pi^+){}^4\text{He}$  by detailed balance. Asterisks: the 50 and 100 MeV  $(\pi^-, n)$  data of Ref. 4 multiplied by 3.25 and 1.7, respectively, as indicated by the  ${}^4\text{He}(\pi^+, p){}^3\text{He}$  data of Ref. 5. Solid line: calculated excitation function at  $t = 0.575 \text{ GeV}^2/c^2$  (from Fig. 4, bottom).

1. P.W.F. Alons, R.D. Bent, J.S. Conte and M. Dillig, Nucl. Phys. A **480** (1988) 413-468.
2. P.W.F. Alons, R.D. Bent and M. Dillig, previous contribution in this Annual Report.
3. J.J. Kehayias, R.D. Bent, M.C. Green, M.A. Pickar and R.E. Pollock, Phys. Rev. C **33** (1986) 725.
4. J. Källne, J.E. Bolger, M.J. Devereaux and S.L. Verbeck, Phys. Rev. C **24** (1981) 1102.
5. J. Källne, R.C. Minehart, R.R. Whitney, R.L. Boudrie, J.B. McClelland and A.W. Setz, Phys. Rev. C **28** (1983) 304.
6. B. Höistad, M. Gazzaly, B. Aas, G. Igo, A. Rahbar, C. Whitten, G.S. Adams and R. Whitney, Phys. Rev. C **29** (1984) 553.
7. J.J. Kehayias, Ph.D. Thesis, Indiana University (1983).
8. D.K. Hasell, A. Bracco, H.P. Gubler, W.P. Lee, W.T.H. van Oers, R. Abegg, D.A. Hutcheon, C.A. Miller, J.M. Cameron, L.G. Greeniaus, G.A. Moss, M.B. Epstein and D.J. Margaziotis, TRIUMF preprint Tri-pp-85-50 (June 1985); D.K. Hasell, Ph.D.

Thesis, University of Manitoba (1983).

9. P.W.F. Alons, E.R. Siciliano and M.J. Leitch, Technical Progress Report 1985, University of Colorado, NPL 1004, p. 2; and P.W.F. Alons, private communication.
10. N. Willis, L. Bimbot, N. Koori, Y. Le Bornec, F. Reide, A. Willis and C. Wilkin, J. Phys. G: Nucl. Phys. **7** (1981) L195.
11. W.R. Falk et al., TRIUMF Experiment No. 413.
12. G.M. Huber, G.J. Lolos, R.D. Bent, K.H. Hicks, P.W. Walden, S. Yen, X. Aslanoglou, E.G. Auld and W.R. Falk, Phys. Rev. **C37** (1988) 1161.
13. G.M. Huber, G.J. Lolos, E.L. Mathie, Z. Papandreou, K.H. Hicks, P.L. Walden, S. Yen, X. Aslanoglou, E.G. Auld and W.R. Falk, Phys. Rev. **C 36** (1987) 1058.
14. J.M. Eisenberg and D.S. Koltun, Theory of Meson Interactions with Nuclei, (John Wiley and Sons, New York, 1980), p. 117.
15. J.V. Noble, Nucl. Phys. **A244** (1975) 526.
16. H.J. Weber and J.M. Eisenberg, Nucl. Phys. **A312** (1978) 201.
17. S.K. Young and W.R. Gibbs, Phys. Rev. **C17** (1978) 837.

## $^{12}\text{C}(p,\pi^+n)$ COINCIDENCE MEASUREMENT

E. Korkmaz\*, S.E. Vigdor, W.W. Jacobs, S.M. Aziz, L.C. Bland, H. Nann,  
*Indiana University Cyclotron Facility, Bloomington, Indiana 47405*

and J.D. Brown

*Department of Physics, Princeton University, Princeton, New Jersey 08554*

A current focus of the IUCF pion production program is on studying the extent to which  $A(p,\pi^\pm)$  reactions can be viewed as resulting from quasifree  $NN \rightarrow NN\pi$  processes in the nucleus.<sup>1,2</sup> Evidence in favor of a quasifree mechanism is particularly striking for  $A(\bar{p},\pi^+)A+1$  reactions, where analyzing power angular distributions  $[A_y(\theta)]$  for continuum production, and for nearly all strong transitions to discrete residual states as well, are similar to results for  $\bar{p}p \rightarrow d\pi^+$ , when the latter are transformed to the nucleon-nucleus reference frame.<sup>1</sup> These  $A_y(\theta)$  are large and negative over most of the angle range. In  $(\bar{p},\pi^+)$  measurements for several lp-shell target nuclei,<sup>1,3</sup> however, we have observed typically one, sometimes two, strong anomalous transitions – to relatively sharp states at high excitation ( $E_x \sim 14\text{-}23$  MeV) – with  $A_y \simeq 0$  at all angles. It is important to understand the nature of the anomalous final states, since these transitions may provide a clue essential to a more complete understanding of pion production from nuclei.

One plausible explanation<sup>1</sup> concerning the anomalous states observed in  $^{12}\text{C}$ ,  $^{13}\text{C}(\bar{p},\pi^+)$  at 21.4 MeV in  $^{13}\text{C}$  and 23.2 MeV in  $^{14}\text{C}$  is that they are isospin-mixed. A  $(p,\pi^+)$  transition to a  $T_>$  state in the final nucleus would involve a  $\Delta T=3/2$  amplitude, which is known<sup>1</sup> from  $(p,\pi^-)$  studies to be characterized by  $A_y$  of opposite sign and of smaller magnitude than is typical for  $\Delta T=1/2$  transitions. A suitable  $T_> - T_<$  admixture could conceivably account for the observed analyzing powers, cross section magnitudes, and